Carbon 157 (2020) 191–200

Contents lists available at ScienceDirect

Carbon

journal homepage: www.elsevier.com/locate/carbon

Development of reversibly compressible feather-like lightweight Chitosan/GO composite foams and their mechanical and viscoelastic properties

Stephanie K. Lee [a], Mei Wang [b], Jin Hyun Lee [c, *], Jonghwan Suhr [a, d, e, **]

[a] Department of Energy Science, Sungkyunkwan University, 2066 Seobu-ro, Jangan-gu, Suwon-si, Gyeonggi-do, 16419, Republic of Korea
[b] State Key Laboratory of Quantum Optics and Quantum Optics Devices, Institute of Laser Spectroscopy, Collaborative Innovation Center of Extreme Optics, Shanxi University, Taiyuan, Shanxi, 030006, China
[c] Polymer Research Center, Inha University, 100 Inha-ro, Michuhol-gu, Incheon, 22212, Republic of Korea
[d] Department of Polymer Science and Engineering, Sungkyunkwan University, 2066, Seobu-ro, Jangan-gu, Suwon-si, Gyeonggi-do, 16419, Republic of Korea
[e] School of Mechanical Engineering, Sungkyunkwan University, 2066 Seobu-ro, Jangan-gu, Suwon-si, Gyeonggi-do, 16419, Republic of Korea

ARTICLE INFO

Article history:
Received 19 June 2019
Received in revised form
30 September 2019
Accepted 11 October 2019
Available online 12 October 2019

ABSTRACT

Three-dimensional (3D) porous materials gain considerable attention in electronics and biomedical/environmental engineering owing to their high porosity, large surface area, and controllable morphological and mechanical properties. In this work, reversibly compressible feather-like lightweight 3D chitosan/graphene oxide (CS/GO) composite foams were prepared with varying the composition ratios of CS to GO using a freeze-drying method. Their structure was obtained via amide linkage formation between the CS amine groups and GO carboxylic acid groups throughout the foam. Chemical analysis of the foams was performed using Fourier-transform infrared spectroscopy, and their morphology was analyzed by field-emission scanning electron microscopy and crosslinking density measurements. Their mechanical features and static and dynamic viscoelastic properties were characterized by monotonic compression, stress-relaxation, and frequency sweep tests using a custom-built micro-indenter and dynamic mechanical analyzer. With increasing the CS concentration, their storage/loss modulus and crosslinking density increased, while their tanδ decreased. Their viscoelastic properties predicted using the proposed modified micromechanics models agreed with the experimental data. This study demonstrates a simple strategy to produce lightweight porous 3D CS/GO composite foams with biocompatibility, electrical conductivity, and decent mechanical and viscoelastic properties regulated by the composition. These foams are promising materials applicable in biomedical and environmental engineering and electrical devices.

1. Introduction

Three-dimensional (3D) hierarchical porous materials, such as aerogels, hydrogels, foams, and sponges, receive significant attention in science and technological fields owing to their unique network structure, low density, and highly developed internal surface area able to provide specific functions [1]. Recently, environmentally friendly, biodegradable, biocompatible, and renewable 3D structural polymer materials have been intensively developed. Synthetic polymers such as poly(vinyl alcohol) [2], poly(ethylene glycol) [3], polyacrylamide [4], and polypeptide [5] and natural polymers such as chitosan (CS) [6], collagen [7], gelatin [8], and alginate [9] are commonly used in biomedical applications owing to their biocompatibility. Among these, CS is a natural linear polysaccharide composed of N-acetyl-D-glucosamine and glucosamine units linked with β-(1–4) bonds and a product of chitin deacetylation derived from the exoskeletons of crustaceans (i.e., crabs, shrimps, crayfishes, etc.) [10–12]. In addition, the polymer chains of CS are easily connected with each other to form porous structures. Moreover, CS has a large number of hydrophilic groups, including amino and hydroxyl groups, which renders it with valuable properties such as biodegradability, biocompatibility,

* Corresponding author.
** Corresponding author. Department of Energy Science, Sungkyunkwan University, 2066 Seobu-ro, Jangan-gu, Suwon-si, Gyeonggi-do, 16419, Republic of Korea.
E-mail addresses: hannahlee@inha.ac.kr (J.H. Lee), suhr@skku.edu (J. Suhr).

https://doi.org/10.1016/j.carbon.2019.10.019
0008-6223/

renewability, nontoxicity, and high chemical resistance. Owing to these advantages, intensive studies have been conducted to investigate the CS-based materials for many applications, including tissue engineering, environmental engineering, drug delivery, wound healing, and biosensors [13–15].

However, the 3D-network structural porous materials consisting of natural polymers, including CS, are typically very brittle and mechanically weak owing to their structural inhomogeneity, which restricts their applications in specific fields [16,17]. Accordingly, the addition of a nano-reinforcement efficiently enhances the mechanical properties as well as physicochemical properties of materials comprising CS [11,12,16,18,19]. In addition, the multifunctional groups (NH_2 and OH groups) in CS facilitate the production of covalent bondings with the functional groups of the reinforcing material [20], thus improving the mechanical strength of the material. The mechanical properties of 3D structural materials depend to a significant extent on the polymer type, processing method, composition, and crosslinking type. In general, their mechanical properties are enhanced by increasing the crosslinking density (ν_c) or introducing nano-sized reinforcing agents (i.e., nanoparticles and nanofibers). For the fabrication of CS-based composite foams, various nano-reinforcements such as carbon nanotubes [21], graphene [22], silica [23], etc. have been employed; furthermore, the enhancement in their mechanical properties was investigated. Note that the chemical modification of nano-reinforcements is typically required to be uniformly dispersed in the polymer matrices [24].

Graphene oxide (GO) that has attracted considerable attention can be used as an ideal nano-reinforcement for polymers because it can improve the chemical, mechanical, and electrical properties of polymer matrices owing to its low density, large surface area, inherent impermeability, high elastic modulus, and conductivity [11,12]. GO is a single atom-layer 2D carbon material arranged in a hexagonal lattice [25] and contains a large number of hydrophilic groups, such as carboxyl, carbonyl, hydroxyl, and epoxy groups. The carboxyl and epoxy groups on the surface of GO sheets facilitate the insertion of small molecules or polymers between its layers via a uniform and stable dispersion of GO in water through hydrogen bonding and electrostatic interaction [12,26,27]. In addition, such multifunctional groups on the surface of GO facilitate a reaction with various polymers having functional groups [28], thus providing a simple fabrication process and unique features such as functionality and amphiphilicity, as compared to well-known nano-reinforcements such as carbon nanotubes and graphene. Moreover, GO has been reported to provide great biocompatibility [29,30]. Therefore, owing to its ideal properties, GO is promising for diverse biomedical applications in addition to electrical and electronic applications.

GO-incorporated CS composite foams were prepared in this study, and the CS/GO foams exhibited an advantageous porosity, structural interconnectivity, and decent mechanical and viscoelastic properties that could be regulated by CS content. In our previous study, we demonstrated the temperature-morphology relationship of CS foams and optimized the synthesis conditions, which facilitated the control of the porous structure of the foam, in addition to focusing on the adsorption properties and biocompatibilities of the foams rather than on their mechanical properties [31]. In this study, we focused on the compressive mechanical behaviors, including the monotonic stress-strain responses and viscoelastic properties of CS/GO composite foams prepared with various compositions, and the relationship with their morphologies was examined. Herein, the biocompatible natural polymer CS with multifunctional groups was used as a primary structural component of the composite foams, while GO was used as a nano-reinforcement to improve the mechanical properties of the foams. A simple freeze-drying method involving a crosslinking process was applied to minimize the chemical decomposition while maintaining a fixed volume and shape of the foams. It was expected that a stable 3D structure would be obtained via the formation of amide linkages between the amine groups of CS and the carboxylic acid groups of GO. Using a custom-built micro-indenter and dynamic mechanical analyzer (DMA), the monotonic compression and static and dynamic viscoelastic properties of the CS/GO foams were measured. The concentration of CS (5, 8, 10, 15, 20, and 40 mg/mL) was varied to investigate the concentration-dependent characteristics of the CS/GO foams and the effect of the ν_c of the CS/GO foams on their mechanical behaviors. By coupling the stress-relaxation tests with the standard linear solid (SLS) model, the static viscoelastic properties of the foams were quantitatively characterized. In addition, frequency sweep tests were performed using DMA to characterize the dynamic viscoelastic behaviors of the foams. The 3D CS/GO composite foams exhibited the concentration-dependent mechanical properties and static and dynamic viscoelastic behaviors. Therefore, the results of this work suggest that the porous CS/GO foams that have morphological and mechanical properties that are controllable and predictable by regulating the foam composition are promising materials for applications in biomedicine, environmental and tissue engineering, and sensors with precise controls.

2. Experimental

2.1. Materials

A CS powder with a medium molecular weight (viscosity = 200–800 cps with 1% acetic acid and deacetylation degree = 75–80%) and acetic acid (ACS reagent; ≥ 99.7%) were purchased from Sigma Aldrich (St. Louis, MO, USA). The aqueous GO dispersion with a concentration of 20 mg/mL (N002-PS-1.0; average thickness = 1.0–1.2 nm, average lateral dimension = 554 nm, and carbon content ≥ 46%) was purchased from Angstron Materials (Dayton, OH, USA). Deionized (DI) water was used as the working fluid throughout all the experiments.

2.2. CS/GO foam fabrication

The CS/GO foams were fabricated using a simple freeze-drying method. The CS solution was prepared by dissolving the CS powder in an aqueous solution of 1 wt% acetic acid (the CS concentrations of 5, 8, 10, 15, 20, and 40 mg/mL). The solution was magnetically stirred until the CS was fully dissolved. The GO suspension was prepared by sonicating a 1 mg/mL aqueous GO dispersion in DI water for 30 min. The CS/GO mixture was prepared by adding the aqueous GO suspension into the CS solution in a volume ratio (CS:GO) of 1:1, followed by sonication. The CS/GO mixture was then poured into 10 mL vials and frozen in a refrigerator at −20 °C. Freeze-drying was then performed at −82 °C for 72 h to obtain the CS/GO foams. The resultant CS/GO foams were weighed, and their densities were determined.

2.3. FT-IR spectroscopy and morphology characterization

A Fourier-transform infrared (FT-IR) spectroscopy analysis was performed using an IR spectrometer (IFS-66/S, TENSOR27, Bruker, MA, USA) to identify the chemical interactions between CS and GO. The scanning was performed in the range of 4000–400 cm^{-1} at a relative scan rate of approximately 110 scan/s. The resolution and wavenumber accuracy were better than 0.1 cm^{-1} and 0.01 cm^{-1}, respectively. The morphologies of the CS/GO foams were analyzed using field-emission scanning electron microscopy (FE-SEM, JSM-

7600F, JEOL Ltd., Japan) at an acceleration voltage of 10 kV. The foams were placed on carbon tapes and pre-treated using Pt plasma before making observations. In parallel, their ν_c values were also determined to investigate their morphology using the following relationship [32,33]:

$$G^{'} = \nu_c RT \quad (1)$$

where R and T denote gas constant and temperature, respectively. G' is the storage modulus, which is determined by DMA, which is discussed in the subsequent sections more explicitly with respect to the viscoelastic properties.

2.4. Mechanical and static viscoelastic characterization and analytical model

Monotonic compression and stress-relaxation tests were performed using a custom-built micro-indenter with a maximum load cell of 10 lb-f. The CS/GO foams were fabricated in cylindrical shapes with average dimensions of approximately 18 mm (diameter) × 13.5 mm (height). A CS/GO foam was placed between two cylindrical indenters with smooth flat plates. The diameters of the cylindrical indenter and chamber were 2.5 and 5 cm, respectively. An initial preload of 0.01 N was applied to the CS/GO foam to ensure full contact between the loading indenter and the foam. The original height of the foam was measured after the application of the preload. The monotonic compression tests were performed according to the American Society for Testing and Materials (ASTM) D1621-10 standard. The foam was compressed to a strain of 80%, which is beyond the purely elastic region, at a loading speed of 10% strain/min; the foam was held compressed for 30 min. The stress-relaxation tests were performed based on the ASTM E328-13 standard. A constant strain of 30% was applied to the foam at a ramp rate of 10% strain/min, and the foam was then held for 40 min. The generalized SLS model, referred to as the generalized Maxwell model, was applied to characterize the static viscoelastic behavior of the foam under compression.

2.5. Dynamic viscoelastic characterization

To characterize the dynamic viscoelastic properties of the CS/GO foams, a DMA 850 instrument (TA Instruments, DE, USA) was used. A cylindrical foam with an average diameter and height of approximately 18 and 6 mm, respectively, was mounted on the DMA fitted with a platen having a diameter of 15 mm at 25 °C. An initial preload of 0.01 N was applied to the foam in order to ensure full contact between the loading platen and the top surface of each foam. After the measurement of the initial height of the foam under the preload, the foam was compressed to a mean strain of 3%, and the crosshead oscillated in a sinusoidal motion. The strain amplitude in the test was 1% while considering an oscillating strain in the range of 2–4%. The strain was maintained in the linear viscous region. Frequency sweep tests were performed for the various CS/GO foams in the range of 0.1–10 Hz.

2.6. Density measurement

The apparent density (ρ) of the CS/GO foam was calculated as follows:

$$\rho = \frac{4W}{\pi d^2 h} \quad (2)$$

where d is the sample diameter (18 mm) and h is the original height. The original height of the foam was determined at the beginning of each measurement. The weight (W) of each foam was measured using an AS 82/220. R2 analytical balance (RADWAG Balances and Scales, Poland).

2.7. Statistical analysis

To evaluate the correlations between the viscoelastic properties (equilibrium modulus, viscous modulus, relaxation time, storage modulus, loss modulus, and loss factor) of the foams, the adjusted R^2 of each calculation was determined, and the linear regression analysis was performed. Outlying experimental data were eliminated in each test. The statistical significance was $P < 0.05$. The p-value of 0.05 (5%) and adjusted $R^2 > 0.8$ indicate that the data are statistically significant.

3. Results and discussion

3.1. Fabrication of 3D CS/GO foams

CS has been extensively analyzed since it has been used as a component of aerogels, hydrogels, scaffolds, foams, and sponges for use in biomedical engineering that needs a porous structure and biodegradability. To investigate the composition-dependent relationship between structure and property, the porous structure in foams, which determines its ability to facilitate the permeation of water or other fluids, was modulated by varying the CS concentrations (5, 8, 10, 15, 20, and 40 mg/mL) where the CS solutions having varied concentrations were mixed with the GO suspension having a fixed concentration of 1 mg/mL.

The fabrication procedure of the CS/GO foams is schematically illustrated in Fig. 1. CS was first dissolved in a 1 wt% aqueous acetic acid solution, thus preparing a uniform yellow solution (Fig. 1a). At this time, various CS solutions having different CS concentrations (5, 8, 10, 15, 20, and 40 mg/mL) were prepared; and the solution became darker in color and thicker in viscosity as the CS concentration increased. A dark brown uniform GO suspension was then prepared by sonicating the GO dispersion in DI water (1 mg/mL) (Fig. 1b). Various CS/GO mixtures were then prepared by adding the aqueous GO suspension into the CS solution with different CS concentration rather than adding the CS solution into the GO suspension and sonicating it (Fig. 1c). This order of the mixing of the solution and suspension is mandatory for the preparation of a stable homogenous dispersion of CS and GO. The reversed order of mixing results in an irreversible agglomeration of GO and is referred to as “bridging” flocculation [34]. A homogeneous CS/GO mixture was first frozen in a refrigerator at −20 °C and then freeze-dried at −82 °C for 3 days (Fig. 1c), according to our previous study [31]. Here, having good control over the freezing temperature is important because the microstructure of the foam is temperature-dependent [31]. This simple freeze-drying process produced the CS/GO foam without damaging its porous structure while maintaining its fixed volume and shape, as shown in Fig. 1.

3.2. Intermolecular interaction mechanism between CS and GO for CS/GO foams

The reaction mechanism between CS and GO is shown in Fig. 2a. The CS/GO foams possess an amorphous network structure that was formed via a significantly strong interaction between CS and GO due to multiple hydrogen and amide bondings [35–38]. When the GO suspension was added to the aqueous solution of CS, the amide covalent bonds were generated between the amino (−NH_2) groups of CS and the carboxyl (−COOH) groups of GO, by acetic acid catalyzed condensation and amidation reactions, along with the hydrogen bonds between hydroxyl and amino groups of CS and

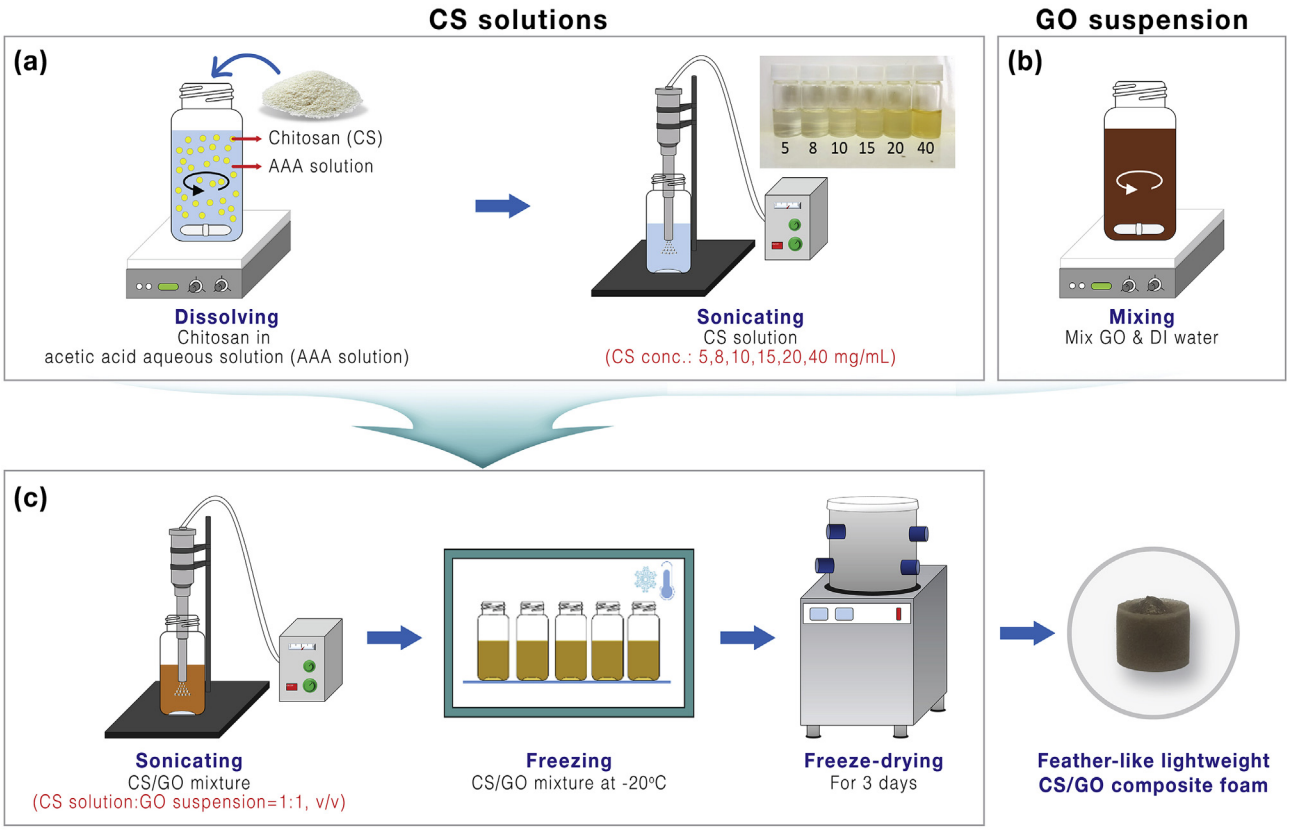

Fig. 1. Schematic of the synthesis procedure of the CS/GO foams: the preparation of the (a) CS solution and (b) GO suspension, and (c) the preparation and freeze-drying the CS/GO mixture and the resulting CS/GO foam. (A colour version of this figure can be viewed online.)

oxygen groups of GO [39,40]. Because GO has the characteristics of large surface area and abundant surface functional groups, even a small amount of GO (1 mg/mL) provided enough functional groups to interact with CS of which concentration increases from 5 to 40 mg/mL.

An FT-IR spectroscopy analysis was perfomed to identify the reaction mechanism and characteristic chemical groups/bonds of the CS/GO foams. The FT-IR spectra of pristine CS and various CS/GO foams prepared with various CS concentrations (5, 8, 10, 15, 20, and 40 mg/mL) are compared in Fig. 2b. The pristine CS exhibits the two characteristic transmittance peaks at 1654 and 1578 cm^{-1} corresponding to the C═O stretching vibration of −NHCO and N−H bending of $-NH_2$, respectively. Various CS/GO foams show similar IR spectra with characteristic peaks at identical wavenumbers (Table S1). The broad peaks in the range of 3450 to 3356 cm^{-1} are attributed to hydrogen bonds and overlap with the stretching vibration peaks of O−H in hydroxyl groups and N−H in amino groups of CS. The peaks at 2920, 2880, and 1404 cm^{-1} are associated with C−H symmetric stretching vibrations. In addition, the transmittance peaks at 1151, 1060, 1028, and 650 cm^{-1} correspond to C−O−C, C−OH, C−OH, and C−O−C symmetric stretching vibrations, respectively. The comparison of the pristine CS and CS/GO foams shows two notable features in the range of 1700 to 1450 cm^{-1} after GO has reacted with the CS. Firstly, the transmittance peaks at 1637 and 1548 cm^{-1} are respectively related to the C═O stretching vibration and N−H bending vibration in the amide bonds formed from the reaction of the primary amino groups of CS with the carboxylic acid groups of GO. Secondly, the characteristic peaks at 1654 cm^{-1} (C═O stretching vibration of −NHCO) and 1578 cm^{-1} (N−H bending vibration) of the CS shift to 1637 cm^{-1} and 1548 cm^{-1}, respectively, for the CS/GO foams, which also indicates the formation of new amide bonds between CS and GO. Moreover, with increasing CS concentration, the intensity of the N−H peaks at 1548 cm^{-1} gradually increase relative to that of the C═O peaks at 1637 cm^{-1}.

3.3. Morphology of the CS/GO foams

Fig. 3 shows the FE-SEM images and photographs of the various CS/GO composite foams under consideration. The CS/GO foams prepared with the CS concentrations of 5, 8, 10, 15, 20, and 40 mg/mL are denoted as CS5/GO1, CS8/GO1, CS10/GO1, CS15/GO1, CS20/GO1, and CS40/GO1, respectively (Table S2), and are cylindrical-shaped and light brown. The foams fabricated with lower CS concentrations exhibit feather-like and more incomplete thinner cell walls, resulting in a softer and more flexible structure with larger porosities and a lower density. Due to the feather-like microstructure of the foams, the pore sizes for lower CS concentrations were not able to measure. The higher CS concentrations yield thicker walls and more homogeneous interconnected pores of the foams, generating a more rigid and stronger structure with smaller porosities, a narrow range of pore size, and a higher density. In other words, the porosities, densities, and pore sizes of the CS/GO foams decrease, increase, and increase, respectively, as the CS concentration increases (Table S2). Therefore, it can be observed that the CS concentration strongly influences the microstructure of the foam.

In addition, the porous structure of the foam is closely associated with the ν_c. By varying the CS concentration, the foams having different degrees of ν_c were obtained using equation (1). It was observed that the G' significantly increased as the CS concentration increases, indicating a higher ν_c. This trend of the G' suggests a more

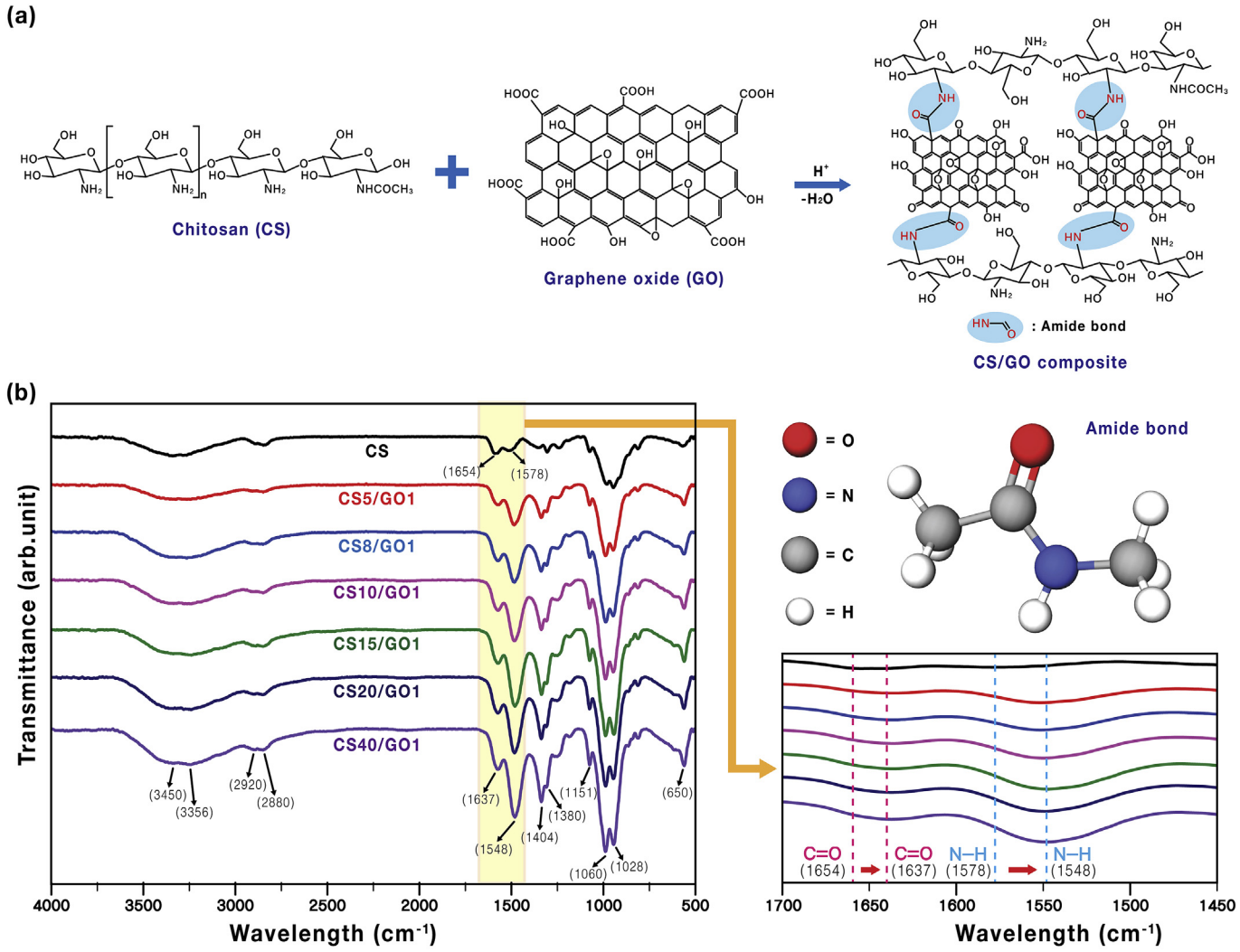

Fig. 2. (a) Schematic of the reaction mechanism between CS and GO to produce CS/GO composite foams. (b) FT-IR spectra of pristine CS and various CS/GO foams prepared with various CS concentrations (5, 8, 10, 15, 20, and 40 mg/mL) (Left). FT-IR-spectra magnified only in the range of wave number from 1450 to 1700 cm^{-1} in order to examine the shift of C═O and N–H bonds for the CS concentrations of the foams (Right). (A colour version of this figure can be viewed online.)

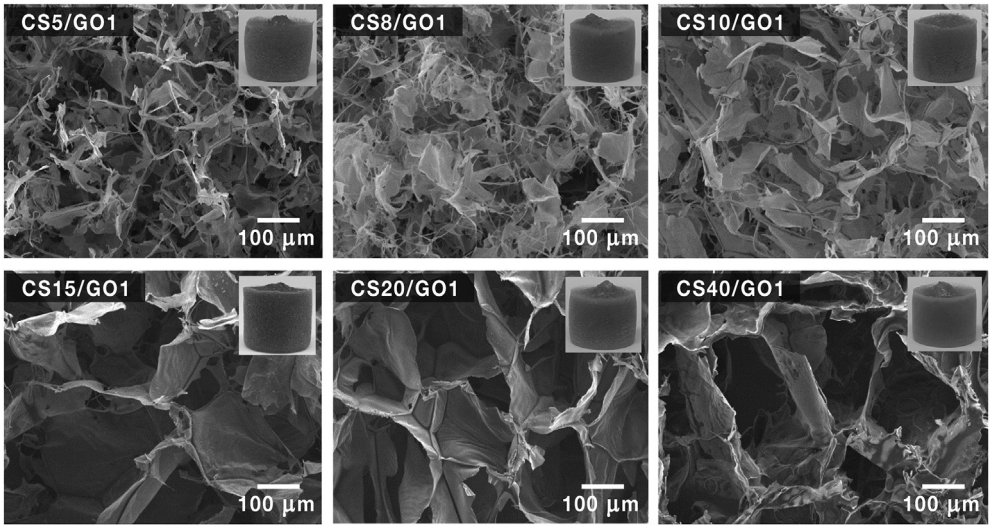

Fig. 3. FE-SEM images and photographs (inset) of the CS/GO foams prepared using various CS concentrations (5, 8, 10, 15, 20, and 40 mg/mL).

compact network structure at higher CS concentrations. Moreover, the porosity of the foams decreased with the increase in the ν_c and CS concentration, in which case, the pore shapes were significantly different among the foams. Furthermore, their apparent density increased exponentially with the CS concentration. Therefore, the ν_c, apparent density, and porosity of the foams are strongly affected by the CS concentration.

3.4. Compressive mechanical properties

A monotonic compression test was performed using a custom-built micro-indenter (Fig. S1) to evaluate the influence of the CS concentration on the compressive strengths and elastic moduli of the CS/GO composite foams. The custom-built micro-indenter is high-sensitive instrumentation controlling the distances and loads; therefore, more accurate property data of the CS/GO foams can be provided. Their stress-strain curves obtained via the excessive monotonic compression tests in the strain range of 0–80% are presented in Fig. 4.

Each CS/GO foam undergoes compression densification without fracture, which is a typically seen in porous foam materials under compression. The stress-strain curve can be classified into three distinct characteristic regions (Fig. 4b): elastic, plateau, and densification regions, which is similar to the deformation behaviors of other foam materials [41–43]. The elastic region corresponds to the linear stress-strain response and elastic bending of the cell walls at low stresses followed by a long collapse plateau and densification. The plateau region represents the regime wherein the stress is dissipated by the plastic deformation that starts and continues until the collapse and buckling of the elastic cell walls. Herein, the energy absorbed per unit volume in the plateau region indicates the energy dissipation capacity. The densification region, where the stress increases sharply as the efficiency of energy dissipation due to the plastic deformation decreases, corresponds to the compaction of the foam. The elastic modulus (E), collapse modulus (E^*), densification modulus (E^{**}), critical strain (ε), densification strain (ε^{**}), and collapse strength (σ^*) of the CS/GO foams, determined using the corresponding stress-strain curves (Fig. 4), are presented in Table 1. In addition, a schematic representation of the compressive stress-strain curve of a foam material for defining the six parameters is shown in Fig. S3.

Table 1
Mechanical properties of the CS/GO foams, including the elastic modulus (E), collapse modulus (E^*), densification modulus (E^{**}), critical strain (ε), densification strain (ε^{**}), and collapse strength (σ^*).

Sample	σ^* (kPa)	ε (%)	ε^{**} (%)	E (kPa)	E^* (kPa)	E^{**} (kPa)
CS5/GO1	0.1728	3.912	68.86	2.107	1.711	39.37
CS8/GO1	0.2312	10.55	68.23	6.835	4.194	110.5
CS10/GO1	0.3891	17.20	67.86	7.931	7.334	193.9
CS15/GO1	7.780	13.30	67.25	55.18	28.52	395.6
CS20/GO1	9.986	11.71	42.60	91.89	50.16	265.3
CS40/GO1	83.39	1.641	7.732	229.7	175.4	673.3

[a] For all of the mechanical properties, the regression analyses show a statistical significance of $P < 0.05$.

The elastic moduli of the CS/GO foams CS5/GO1, CS8/GO1, CS10/GO1, CS15/GO1, CS20/GO1, and CS40/GO1 were 2.107, 6.835, 7.931, 55.18, 91.89, and 229.7 kPa, respectively, while their compressive strengths were 0.1728, 0.2312, 0.3891, 7.780, 9.986, and 83.39 kPa, respectively. The comparison of CS5/GO1 and CS40/GO1 shows that the elastic modulus and compressive strength exhibit a significant increment of approximately 10,788% and 47,250%, respectively, with the increase in the CS concentration from 5 to 40 mg/mL. This is because CS40/GO1 has a stronger and more rigid microstructure, which is most probably because of the higher CS concentration results in the very strong interactions between CS and GO. From these results, it can be inferred that the CS concentration effectively influences the mechanical properties of the CS/GO foams. Here, a regression analysis confirms the significant statistical difference in the mechanical properties (elastic modulus, collapse modulus, densification modulus, and collapse strength) between the foams ($P < 0.05$).

3.5. Static viscoelastic properties and analytical model

A stress-relaxation test was carried out to evaluate the static viscoelastic behaviors of the CS/GO foams under a constant compressive strain of 30% at 25 °C. The typical stress-relaxation responses of the foams prepared with different CS concentrations (from 5 to 40 mg/mL) are presented in Fig. 5a. The stress gradually decreases over time and finally reaches the equilibrium state, which reflects the static viscoelastic properties. The equilibrium

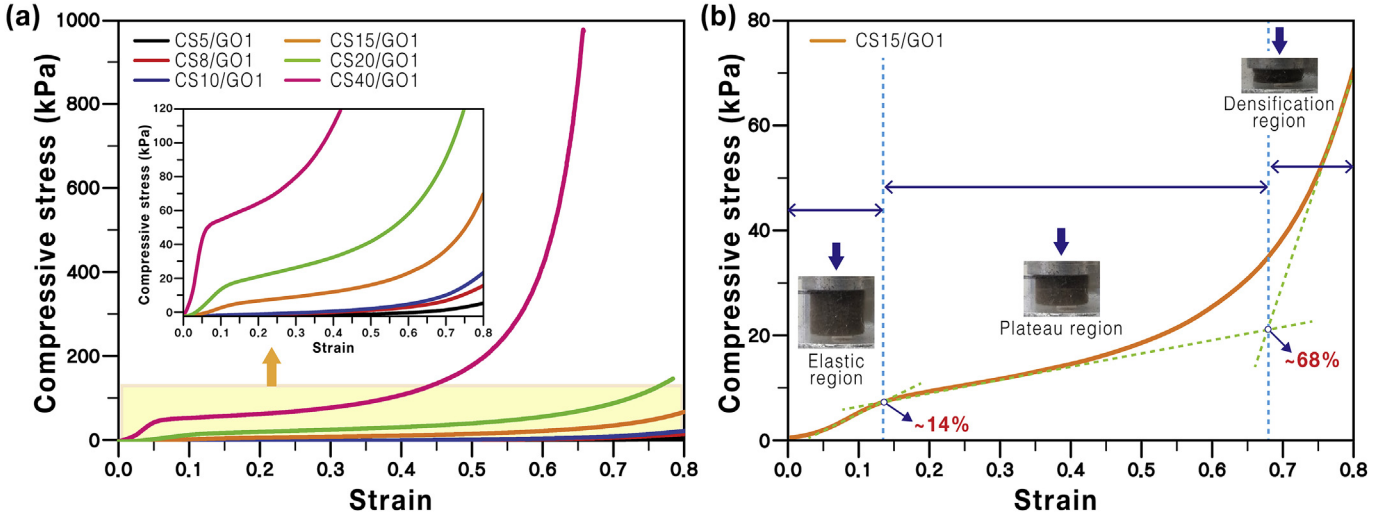

Fig. 4. (a) Uniaxial compressive stress-strain curves of the CS/GO foams prepared using various CS concentrations (5, 8, 10, 15, 20, and 40 mg/mL) in the strain range of 0–80%. (b) Stress-strain curve of CS15/GO1. The linear elastic region (~14%), plateau region (14%–68%), and densification region (68%~) are denoted using dotted lines and solid blue arrows. (A colour version of this figure can be viewed online.)

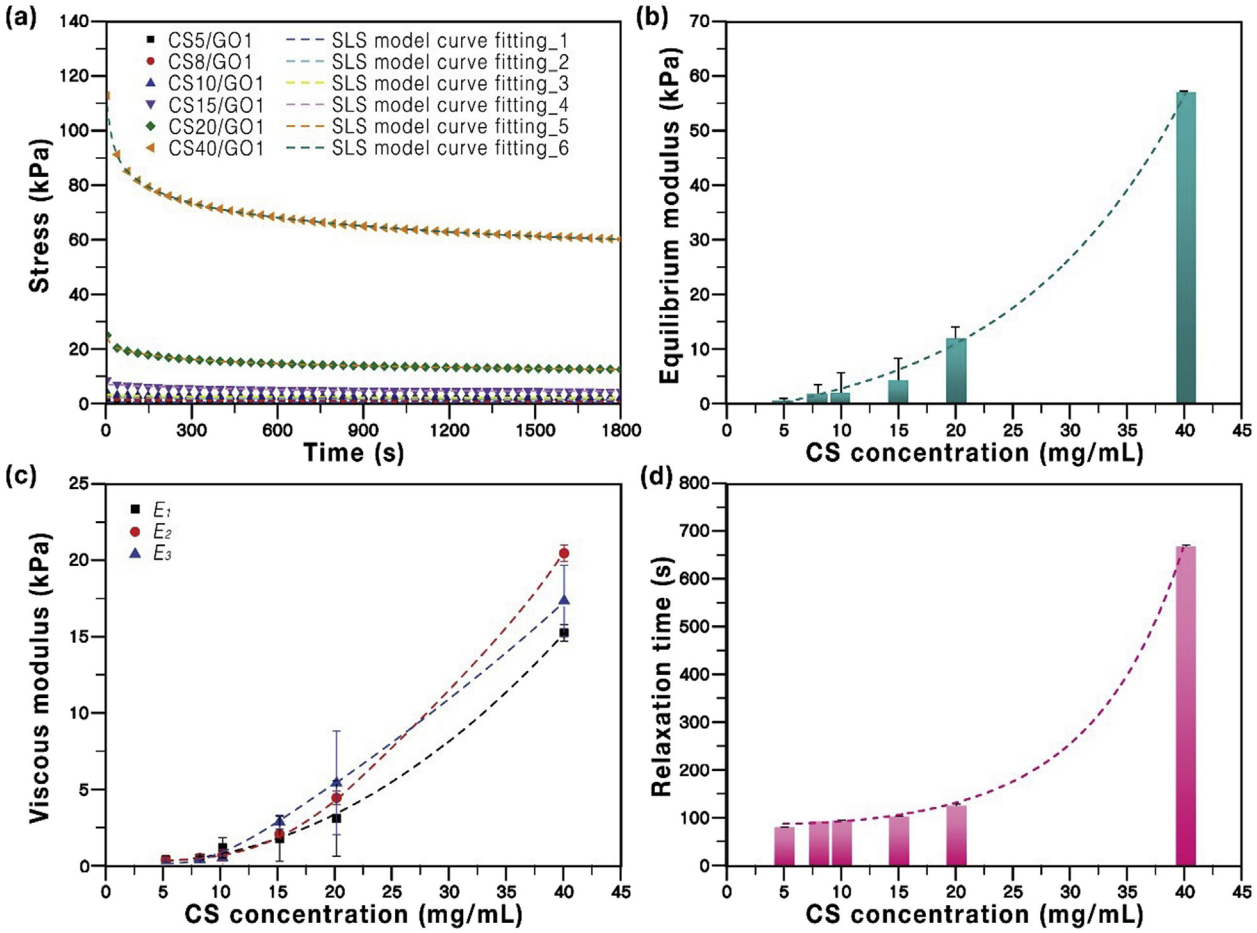

Fig. 5. Static viscoelastic properties of the CS/GO foams: (a) Stress-relaxation behavior of the CS/GO foams under a constant strain deformation of 30%. The stress-relaxation response was fitted with the generalized Maxwell model (equation (3)). (b) Equilibrium moduli (E_∞) and (c) viscous moduli (E_1, E_2, and E_3) of the CS/GO foams determined by fitting curves drawn using the generalized Maxwell model. (d) Relaxation time (τ) of the CS/GO foams obtained for the time at which the stress relaxes to $1/e$ of its initial value. (A colour version of this figure can be viewed online.)

modulus, viscous modulus, and relaxation time were determined by characterizing the stress-relaxation curves obtained using a generalized SLS model. The SLS model was employed to characterize the viscoelastic behaviors of the CS/GO foams under compression. The Maxwell model is often used as an SLS model to describe the stress-relaxation behavior, with a linear combination of the elastic and viscous components represented by springs and dashpots. In this study, the modified Maxwell model with four springs and three dashpots in series (Fig. S2) was employed, which is expressed as follows:

$$\sigma(t) = E_\infty + E_1 e^{-\frac{t}{\tau_1}} + E_2 e^{-\frac{t}{\tau_2}} + E_3 e^{-\frac{t}{\tau_3}} \quad (3)$$

where E_∞ is the equilibrium modulus representing the elastic modulus of the long-term spring element; E_1, E_2, and E_3 are the viscous moduli representing the elastic moduli of the springs; and τ_1, τ_2, and τ_3 are the relaxation times of the dashpots. The model takes into consideration that relaxation occurs at a set of time moments and not in a single time moment. It is clearly observed that this modified Maxwell model fits the experimental data well (Fig. 5a). The values of the equilibrium modulus (E_∞), viscous moduli (E_1, E_2, and E_3), and relaxation time (τ, time constant where the stress is relaxed to $1/e$ of the initial value) were determined by using curve fitting (Fig. 5b–d), and the determined values are presented in Table 2.

In general, when porous elastic materials such as foams, sponges, and scaffolds are under compression, the air inside the network is forced out during the deformation. Thus, the porous elastic materials exhibit the flow-dependent viscoelastic behaviors that are affected primarily by the interaction between the porous solid network and the airflow [44,45]. The viscoelastic properties of the CS/GO foams were correlated with their apparent density and porosity, which was closely correlated with the CS concentration. The determined viscoelastic properties of the CS/GO foams are enhanced by increasing the CS concentration. Three significant consequences are noticeable. Firstly, the equilibrium modulus, indicating the stiffness, of the CS/GO foams increases as the CS concentration increases. CS40/GO1 exhibits the highest equilibrium modulus (57.11 kPa) as expected, and CS20/GO1, CS15/GO1, CS10/GO1, and CS8/GO1 exhibit moderate values in the range of 11.89 to 1.688 kPa, while CS5/GO1 exhibits the lowest value of 0.5961 kPa. Secondly, the higher CS concentrations resulted in a smaller porosity in the foam owing to the larger friction force between the solid network and air, thus inducing a higher viscous modulus. The highest viscous moduli of the CS40/GO1 are most probably caused by the relatively thicker and more rigid walls of the network cells (refer to Fig. 3), which induces larger viscous friction forces between the airs or between air and the wall against the applied compressive force. Furthermore, the lowest viscous moduli of the CS5/GO1 are probably due to the relatively softer and more flexible

Table 2
Equilibrium moduli (E_∞), viscous moduli (E_1, E_2, and E_3), and relaxation times (τ_1, τ_2, and τ_3) of the CS/GO foams prepared using various CS concentrations (5, 8, 10, 15, 20, and 40 mg/mL).

Sample	E_∞ (kPa)	E_1 (kPa)	E_2 (kPa)	E_3 (kPa)	τ_1 (s)	τ_2 (s)	τ_3 (s)	$\overline{R^2}$
CS5/GO1	0.5961	0.1986	0.1132	0.2133	1343	33.82	33.82	0.9909
CS8/GO1	1.688	0.2714	0.4611	0.3101	52.28	832.9	832.8	0.9985
CS10/GO1	2.062	0.9843	0.6024	0.5206	1896	110.0	1896	0.9964
CS15/GO1	4.748	3.308	1.657	0.5653	444.3	444.3	444.3	0.9699
CS20/GO1	11.89	5.350	2.987	4.372	1016	11.92	141.7	0.9999
CS40/GO1	57.11	15.26	16.38	20.53	124.4	19.69	966.7	0.9997

[a] The adjusted R^2 is a statistical measure representing the percentage of variation attributed to only those independent variables that affect the dependent variable.
[b] All values were determined using a generalized Maxwell model.

wall of the cells (refer to Fig. 3), which result in smaller viscous friction forces. Thirdly, the time required for the dissipation of the air entrapped in the foams increases with the CS concentration, which corresponds to longer relaxation time. CS40/GO1 exhibits a significantly larger relaxation time than those of the other foams. CS40/GO1, CS20/GO1, CS15/GO1, CS10/GO1, CS8/GO1, and CS5/GO1 exhibit relaxation times of 670.1, 98.25, 80.30, 76.26, 36.24, and 23.44 s, respectively. For the same applied strain, the built-up stress level of CS40/GO1 increased, and thus, a significantly longer time was required to release the step load.

3.6. Dynamic viscoelastic properties

In addition to the static viscoelastic properties of the CS/GO foams, their dynamic viscoelastic properties were characterized by DMA in a wide frequency range of 0.1–10 Hz at 25 °C. Fig. 6a presents the G' of the foams, which characterizes the ability of the foam to store deformation energy in the elastic regime. The G' slightly increases with increasing frequency in the range of 0.1–10 Hz. CS40/GO1 exhibits the highest G' of approximately 1490 kPa at 0.1 Hz, and its G' gradually increases up to 2618 kPa with increasing frequency. In contrast, CS5/GO1 shows the lowest G' values of 8.810–12.84 kPa and moderately increases with frequency. The G' values of CS40/GO1 are two orders of magnitude higher than those of CS5/GO1, which implies the CS concentration-dependent elastic behavior.

Loss modulus (G'') that reflects the dissipated energy and viscous response of material was examined for the CS/GO foams. Fig. 6b shows the G'' of the foams as a function of frequency. In contrast to their G', their G'' slightly decreases with increasing frequency. In general, when the elastic contribution (i.e., G') of a material system increases, the system becomes less viscous and dissipates a smaller amount of energy (i.e., smaller G'') with the increase in the frequency. However, the G'' and G' of the CS/GO foams increase with the CS concentration, meaning that the foams become more elastic and concurrently dissipate more energy for the higher CS concentration. CS40/GO1 exhibits the highest G'' of 302.2 kPa at 0.1 Hz, which decreases to 166.8 kPa at 10 Hz, while CS5/GO1 exhibits the lowest G'' values of 1.112 to 0.8963 kPa. The G'' values of CS40/GO1 are two orders of magnitude higher than those of CS5/GO1. These results confirm that the viscous feature of CS/GO foams is concentration-dependent.

The loss factor ($\tan\delta$) of the foams, which is the ratio of the G'' to the G', was also determined to characterize the viscous-to-elastic behavior of the foams. In general, the intensity of the maximum $\tan\delta$ peak of polymers represents the extent of their mobility [46]; a higher value of $\tan\delta$ indicates their higher energy dissipation and more viscous behavior whereas a lower value indicates their less viscous and higher elastic behavior. Fig. 6c presents the $\tan\delta$ value of the maximum $\tan\delta$ peak of the foams with increasing frequency. The $\tan\delta$ values decrease as the CS concentration increases, which can be explained by the fact that a higher content of CS in the foam probably produces a higher ν_c, thus resulting in a greater restriction in the mobility of polymer molecular chains.

The normalized G' and normalized $\tan\delta$ of the foams that were determined as a function of the CS concentration at 1 Hz to normalize the G' and $\tan\delta$ without an apparent density effect are presented in Fig. 6d. The $\tan\delta$ decreases with the increases in the CS concentration, while the G' increases, which confirms that the foams are more elastic than viscous upon the application of the load. It is also implied that the foams are more likely to store the loaded energy than to dissipate it. The $\tan\delta$ decreases from 17.75 to 4.162 cm^3/g with the increase in the CS concentration from 5 to 40 mg/mL. The increase in the CS content in the foams restricts the molecular movement of the polymer chains in the network, which results in more elastic material response, and also causes $\tan\delta$ to decrease, which improves the dissipation capability of the CS/GO foam.

Fig. 6e shows that both the G' and ν_c increase with the increase in the CS concentration. The increase in the CS concentration strengthens the interaction among the CS and GO molecules, which densifies the polymer network and enhances the mechanical stiffness of the foam. The ν_c of the foams was determined according to the direct relation of the G' of the network materials with their ν_c, as represented in equation (1). The result that the increasing tendency of the G' and ν_c with the increase in the CS concentration are the above relationship. CS40/GO1 shows the greatest ν_c and G' (mechanical rigidity). The fact that the G' increases with the frequency because polymer chains in the network have a shorter time to relax the applied stress indicates that the most rigid CS40/GO1 foam requires a longer time to release the loaded stress.

According to the cumulative results, the dynamic viscoelastic properties, including the G', G'', and $\tan\delta$, and the morphology such as ν_c, which are dependent on the CS concentration, of the CS/GO foams are illustrated in Fig. 6f. Their G', G'', and ν_c increase with the increase in the CS concentration, while their $\tan\delta$ decrease. In addition, the illustration of the foam network structure with lower and higher ν_c demonstrates that the crosslinks formed by the interaction between CS and GO become looser and denser, respectively, for the lower and higher CS concentrations. Therefore, similar to the static behaviors affected by the CS concentration, the dynamic viscoelastic properties of the foams were also observed to be dependent on the CS concentration.

4. Conclusions

Using a simple freeze-drying approach that induces a crosslinking process, reversibly compressible feather-like lightweight 3D CS/GO composite foams were fabricated by mixing a GO suspension and a CS solution with varying CS concentrations. The CS concentration had a significant influence on the network morphologies (i.e., crosslinking density and pore structure) and mechanical and viscoelastic characteristics of the CS/GO foams. The foams prepared

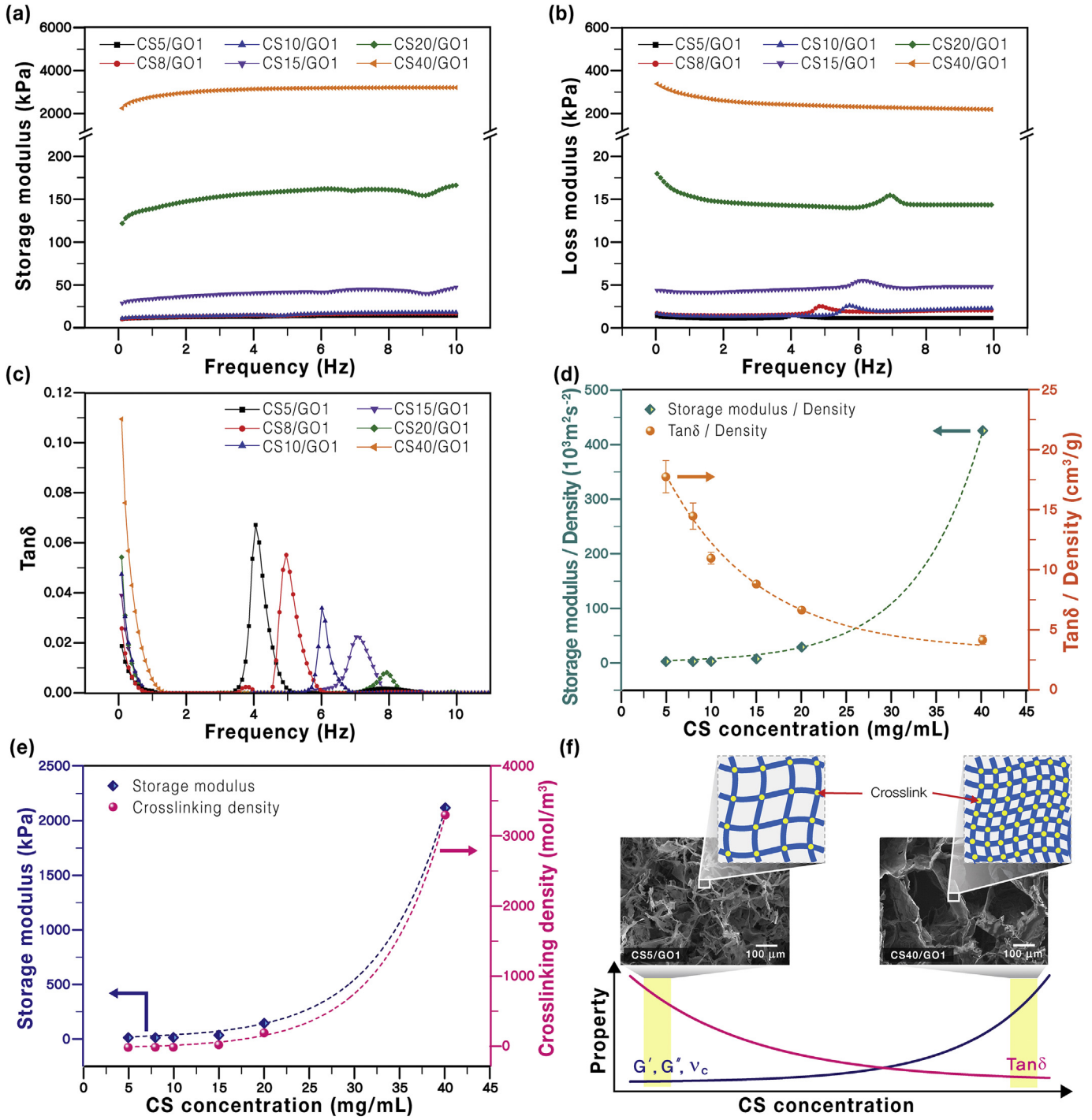

Fig. 6. Dynamic viscoelastic properties of the CS/GO foams: (a) Storage moduli (G'), (b) loss moduli (G''), and (c) loss factor (tanδ) of the CS/GO foams as a function of the frequency at a mean strain of 3% and strain amplitude of 1%. (d) Density-normalized G' and tanδ values of the CS/GO foams prepared using various CS concentrations. (e) Relationships between the G' and crosslinking density (ν_c) of the CS/GO foams with the different CS concentrations. (f) Correlation of the dynamic viscoelastic properties (i.e., G', G'', and tanδ) and ν_c (expected crosslinked network structure) for the different concentrations of CS. (A colour version of this figure can be viewed online.)

with a lower CS concentration yielded a lower crosslinking density and a softer and more flexible structure having a smaller elastic modulus, while the foams prepared with a higher CS concentration produced a higher crosslinking density and a stronger and more rigid structure having a greater elastic modulus. The monotonic compression responses of the CS/GO foams showed that their elastic modulus and compressive strength were significantly enhanced as the CS concentration increased, and the maximum elastic modulus and compressive strength were measured as 229.7 kPa and 83.39 kPa, respectively, at the highest CS concentration. Their stress-relaxation behaviors could be explained by the generalized Maxwell model with four springs and three dashpots in series. Moreover, the equilibrium moduli, viscous moduli, and relaxation times increased with the increase in the CS concentration. With respect to the dynamic viscoelastic behaviors of the CS/GO foams, the storage modulus gradually increased with the

frequency in the range of 0.1–10 Hz, while the loss modulus decreased. The foams also exhibited the CS concentration-dependent behaviors: the storage and loss moduli increased with the increase in the CS concentration, while the value and intensity of the maximum tanδ peak decreased with the increasing CS content. This study provides a strategy for the design and fabrication of 3D CS/GO composite foams, which possess biocompatibility and electrical conductivity and desirable mechanical and viscoelastic properties that can be regulated by the network structure and composition, as promising materials for various applications including intelligent materials, electrical devices, and biomedical and environmental engineering.

Declaration of competing interest

The authors declare that they have no known competing financial interests or personal relationships that could have appeared to influence the work reported in this paper.

Acknowledgements

This study was supported by the National Research Foundation of Korea, which is grant-funded by the Korea government (MSIP; Ministry of Science, ICT & Future Planning) (No. 2018R1A2B2001565).

Appendix A. Supplementary data

Supplementary data to this article can be found online at https://doi.org/10.1016/j.carbon.2019.10.019.

References

[1] G.M. Vladimirovich, V.P. Melnikov, Graphene Oxide/Reduced Graphene Oxide Aerogels. Graphene Oxide-Applications and Opportunities, IntechOpen, 2018.
[2] M. Guvendiren, J.A. Burdick, Engineering synthetic hydrogel microenvironments to instruct stem cells, Curr. Opin. Biotechnol. 24 (5) (2013) 841–846.
[3] J. Zhu, Bioactive modification of poly (ethylene glycol) hydrogels for tissue engineering, Biomaterials 31 (17) (2010) 4639–4656.
[4] L.H. Christensen, V.B. Breiting, A. Aasted, A. Jørgensen, I. Kebuladze, Long-term effects of polyacrylamide hydrogel on human breast tissue, Plast. Reconstr. Surg. 111 (6) (2003) 1883–1890.
[5] P. Markland, Y. Zhang, G.L. Amidon, V.C. Yang, A pH-and ionic strength-responsive polypeptide hydrogel: synthesis, characterization, and preliminary protein release studies, J. Biomed. Mater. Res. 47 (4) (1999) 595–602.
[6] M. Dash, F. Chiellini, R.M. Ottenbrite, E. Chiellini, Chitosan—a versatile semi-synthetic polymer in biomedical applications, Prog. Polym. Sci. 36 (8) (2011) 981–1014.
[7] X. Liu, C. Zheng, X. Luo, X. Wang, H. Jiang, Recent advances of collagen-based biomaterials: multi-hierarchical structure, modification and biomedical applications, Mater. Sci. Eng. C 99 (2019) 1509–1522.
[8] J.-P. Draye, B. Delaey, A. Van de Voorde, A. Van Den Bulcke, B. De Reu, E. Schacht, In vitro and in vivo biocompatibility of dextran dialdehyde cross-linked gelatin hydrogel films, Biomaterials 19 (18) (1998) 1677–1687.
[9] G. Orive, S. Ponce, R. Hernandez, A. Gascon, M. Igartua, J. Pedraz, Biocompatibility of microcapsules for cell immobilization elaborated with different type of alginates, Biomaterials 23 (18) (2002) 3825–3831.
[10] S. Islam, M.R. Bhuiyan, M. Islam, Chitin and chitosan: structure, properties and applications in biomedical engineering, J. Polym. Environ. 25 (3) (2017) 854–866.
[11] S. Sayyar, E. Murray, B. Thompson, J. Chung, D.L. Officer, S. Gambhir, G.M. Spinks, G.G. Wallace, Processable conducting graphene/chitosan hydrogels for tissue engineering, J. Mater. Chem. B 3 (3) (2015) 481–490.
[12] X. Jing, H.-Y. Mi, B.N. Napiwocki, X.-F. Peng, L.-S. Turng, Mussel-inspired electroactive chitosan/graphene oxide composite hydrogel with rapid self-healing and recovery behavior for tissue engineering, Carbon 125 (2017) 557–570.
[13] I.-Y. Kim, S.-J. Seo, H.-S. Moon, M.-K. Yoo, I.-Y. Park, B.-C. Kim, C.-S. Cho, Chitosan and its derivatives for tissue engineering applications, Biotechnol. Adv. 26 (1) (2008) 1–21.
[14] S.K.L. Levengood, M. Zhang, Chitosan-based scaffolds for bone tissue engineering, J. Mater. Chem. B 2 (21) (2014) 3161–3184.
[15] S. Saravanan, R. Leena, N. Selvamurugan, Chitosan based biocomposite scaffolds for bone tissue engineering, Int. J. Biol. Macromol. 93 (2016) 1354–1365.
[16] S. Deepthi, J. Venkatesan, S.-K. Kim, J.D. Bumgardner, R. Jayakumar, An overview of chitin or chitosan/nano ceramic composite scaffolds for bone tissue engineering, Int. J. Biol. Macromol. 93 (2016) 1338–1353.
[17] D. Han, L. Yan, W. Chen, W. Li, Preparation of chitosan/graphene oxide composite film with enhanced mechanical strength in the wet state, Carbohydr. Polym. 83 (2) (2011) 653–658.
[18] E. Bolaina-Lorenzo, C. Martínez-Ramos, M. Monleón-Pradas, W. Herrera-Kao, J.V. Cauich-Rodríguez, J.M. Cervantes-Uc, Electrospun polycaprolactone/chitosan scaffolds for nerve tissue engineering: physicochemical characterization and Schwann cell biocompatibility, Biomed. Mater. 12 (1) (2016), 015008.
[19] B. Choi, S. Kim, B. Lin, B.M. Wu, M. Lee, Cartilaginous extracellular matrix-modified chitosan hydrogels for cartilage tissue engineering, ACS Appl. Mater. Interfaces 6 (22) (2014) 20110–20121.
[20] S.K. Shukla, A.K. Mishra, O.A. Arotiba, B.B. Mamba, Chitosan-based nanomaterials: a state-of-the-art review, Int. J. Biol. Macromol. 59 (2013) 46–58.
[21] Y. Li, M. Zhao, J. Chen, S. Fan, J. Liang, L. Ding, S. Chen, Flexible chitosan/carbon nanotubes aerogel, a robust matrix for in-situ growth and non-enzymatic biosensing applications, Sens. Actuators B Chem. 232 (2016) 750–757.
[22] H. Yuan, L.-Y. Meng, S.-J. Park, A review: synthesis and applications of graphene/chitosan nanocomposites, Carbon Letters 17 (1) (2016) 11–17.
[23] Q. Ma, Y. Liu, Z. Dong, J. Wang, X. Hou, Hydrophobic and nanoporous chitosan–silica composite aerogels for oil absorption, J. Appl. Polym. Sci. 132 (15) (2015) 41770.
[24] M. Šupová, G.S. Martynková, K. Barabaszová, Effect of nanofillers dispersion in polymer matrices: a review, Sci. Adv. Mater. 3 (1) (2011) 1–25.
[25] A.K. Geim, A.H. MacDonald, Graphene: exploring carbon flatland, Phys. Today 60 (8) (2007) 35–41.
[26] D.R. Dreyer, S. Park, C.W. Bielawski, R.S. Ruoff, The chemistry of graphene oxide, Chem. Soc. Rev. 39 (1) (2010) 228–240.
[27] S. Pei, H.-M. Cheng, The reduction of graphene oxide, Carbon 50 (9) (2012) 3210–3228.
[28] Y. Zhu, S. Murali, W. Cai, X. Li, J.W. Suk, J.R. Potts, R.S. Ruoff, Graphene and graphene oxide: synthesis, properties, and applications, Adv. Mater. 22 (35) (2010) 3906–3924.
[29] L. Pang, C. Dai, L. Bi, Z. Guo, J. Fan, Biosafety and antibacterial ability of graphene and graphene oxide in vitro and in vivo, Nanoscale. Res. Lett. 12 (1) (2017) 564.
[30] M. Skoda, I. Dudek, A. Jarosz, D. Szukiewicz, Graphene: one material, many possibilities—application difficulties in biological systems, J. Nanomater. 2014 (2014) 190.
[31] M. Wang, Y. Ma, Y. Sun, S.Y. Hong, S.K. Lee, B. Yoon, L. Chen, L. Ci, J.-D. Nam, X. Chen, J. Suhr, Hierarchical porous chitosan sponges as robust and recyclable adsorbents for anionic dye adsorption, Sci. Rep. 7 (1) (2017) 18054.
[32] A. Hajighasem, K. Kabiri, Cationic highly alcohol-swellable gels: synthesis and characterization, J. Polym. Res. 20 (8) (2013) 218.
[33] H. Jiang, W. Su, P.T. Mather, T.J. Bunning, Rheology of highly swollen chitosan/polyacrylate hydrogels, Polymer 40 (16) (1999) 4593–4602.
[34] M. Fang, J. Long, W. Zhao, L. Wang, G. Chen, pH-responsive chitosan-mediated graphene dispersions, Langmuir 26 (22) (2010) 16771–16774.
[35] A.S.K. Kumar, S.-J. Jiang, Chitosan-functionalized graphene oxide: a novel adsorbent an efficient adsorption of arsenic from aqueous solution, J. Environ. Chem. Eng. 4 (2) (2016) 1698–1713.
[36] X. Qian, N. Li, Q. Wang, S. Ji, Chitosan/graphene oxide mixed matrix membrane with enhanced water permeability for high-salinity water desalination by pervaporation, Desalination 438 (2018) 83–96.
[37] A. Singh, G. Sinsinbar, M. Choudhary, V. Kumar, R. Pasricha, H. Verma, S.P. Singh, K. Arora, Graphene oxide-chitosan nanocomposite based electrochemical DNA biosensor for detection of typhoid, Sens. Actuators B Chem. 185 (2013) 675–684.
[38] Y. Zhang, M. Zhang, H. Jiang, J. Shi, F. Li, Y. Xia, G. Zhang, H. Li, Bio-inspired layered chitosan/graphene oxide nanocomposite hydrogels with high strength and pH-driven shape memory effect, Carbohydr. Polym. 177 (2017) 116–125.
[39] F. Emadi, A. Amini, A. Gholami, Y. Ghasemi, Functionalized graphene oxide with chitosan for protein nanocarriers to protect against enzymatic cleavage and retain collagenase activity, Sci. Rep. 7 (2017) 42258.
[40] K. Bustos-Ramírez, A.L. Martínez-Hernández, G. Martínez-Barrera, M.D. Icaza, V.M. Castaño, C. Velasco-Santos, Covalently bonded chitosan on graphene oxide via redox reaction, Materials 6 (3) (2013) 911–926.
[41] M. Ashby, L. Gibson, Cellular Solids: Structure and Properties, Press Syndicate of the University of Cambridge, Cambridge, UK, 1997, pp. 175–231.
[42] M. Avalle, G. Belingardi, R. Montanini, Characterization of polymeric structural foams under compressive impact loading by means of energy-absorption diagram, Int. J. Impact Eng. 25 (5) (2001) 455–472.
[43] T.H. Courtney, Mechanical Behavior of Materials, Waveland Press, 2005.
[44] Y. Kameo, T. Adachi, M. Hojo, Transient response of fluid pressure in a poroelastic material under uniaxial cyclic loading, J. Mech. Phys. Solids 56 (5) (2008) 1794–1805.
[45] W. Zhao, A.L. Elias, L.P. Rajukumar, H.I. Kim, D.J. O'Brien, B.K. Zimmerman, E.S. Penev, M. Terrones, B.I. Yakobson, B. Wei, Controllable and predictable viscoelastic behavior of 3D boron-doped multiwalled carbon nanotube sponges, Part. Part. Syst. Charact. 33 (1) (2016) 21–26.
[46] D.J.T. Hill, M.C.S. Perera, P.J. Pomery, H.K. Toh, Dynamic mechanical properties of networks prepared from siloxane modified divinyl benzene pre-polymers, Polymer 41 (26) (2000) 9131–9137.